2022

Improving the Holographic Recording Characteristics of a Water-Resistant Photosensitive Sol–Gel for Use in Volume Holographic Optical Elements

Brian Rogers
Technological University Dublin, brian.rogers@tudublin.ie

Tatsiana Mikulchyk
Technological University Dublin, tatsiana.mikulchyk@tudublin.ie

Mohamed Oubaha
Technological University Dublin, mohamed.oubaha@tudublin.ie

See next page for additional authors

Recommended Citation

Rogers, B., Mikulchyk, T. & Oubaha, M. (2022). Improving the Holographic Recording Characteristics of a Water-Resistant Photosensitive Sol–Gel for Use in Volume Holographic Optical Elements. *Photonics*, vol. 9, no. 636 doi:10.3390/photonics9090636

photonics

MDPI

Article

Improving the Holographic Recording Characteristics of a Water-Resistant Photosensitive Sol–Gel for Use in Volume Holographic Optical Elements

Brian Rogers [1,2], Tatsiana Mikulchyk [1,2], Mohamed Oubaha [2,3], Dervil Cody [1,2], Suzanne Martin [1,2] and Izabela Naydenova [1,2,*]

[1] Centre for Industrial and Engineering Optics, School of Physics, Clinical and Optometric Sciences, Technological University Dublin (TU Dublin), D07 ADY7 Dublin, Ireland
[2] FOCAS Research Institute, Technological University Dublin (TU Dublin), 13 Camden Row, D08 CKP1 Dublin, Ireland
[3] Centre for Research in Engineering and Surface Technology (CREST), Technological University Dublin (TU Dublin), 13 Camden Row, D08 CKP1 Dublin, Ireland
* Correspondence: izabela.naydenova@tudublin.ie

Abstract: Continual improvements to holographic recording materials make the development of volume holographic optical elements increasingly more attainable for applications where highly efficient, lightweight diffractive optical elements can replace conventional optics. A fast-curing, water resistant photosensitive sol–gel capable of volume holographic recording has recently drawn attention for its extreme environmental and physical robustness, in particular its water/moisture and scratch resistance. However, to date, the refractive index modulation has been limited. While water-resistant properties are invaluable in the face of the weathering which many practical systems for outdoor applications will endure, high refractive index modulation is also important in order to facilitate high diffraction efficiency holograms recorded in relatively thin layers. Lower grating thickness ensures a large angular and wavelength range of operation-properties that are critical for many applications of holographic optical elements such as solar light harvesting, optical displays and illumination management. For any application where low-cost mass production is envisaged, sensitivity/writing speed is also a crucial factor. In this research, we studied the recording properties of these water-resistant photosensitive sol–gel layers at two different recording wavelengths (532 and 476 nm) and investigated methods for improving these properties. We report more than two-fold improvement of the refractive index modulation from 1.4×10^{-3} to 3.3×10^{-3} in layers of thickness ranging from 40–100 μm and more than an order of magnitude increase in photosensitivity/recording speed through better matching between recording wavelength and layer absorption, chemical alterations and thermal post-processing techniques.

Keywords: holography; sol–gel; optical materials; holographic optical element

Citation: Rogers, B.; Mikulchyk, T.; Oubaha, M.; Cody, D.; Martin, S.; Naydenova, I. Improving the Holographic Recording Characteristics of a Water-Resistant Photosensitive Sol–Gel for Use in Volume Holographic Optical Elements. *Photonics* **2022**, *9*, 636. https://doi.org/10.3390/photonics9090636

Received: 14 July 2022
Accepted: 2 September 2022
Published: 4 September 2022

1. Introduction

Recent improvements in photopolymer holographic materials [1] have led to new developments in holographic optical elements (HOEs). Volume photopolymer HOEs [2,3] offer a significant improvement in surface elements since they can be patterned (with low intensity exposure) [4] through the volume of the materials, can be laminated [5,6] into a stack and, importantly, can achieve near 100% re-direction of incident light into a single output beam [7,8]. This optical patterning can potentially replace the etching and stamping process associated with stamped diffractive optics and can facilitate customisation and small batches. Very high fringe-slant and diffraction angles are also achievable in these materials [9,10]. The key applications currently envisaged for such elements are solar collection, displays and light management.

Holographic optical elements for solar concentration have been tested in different systems and studied by numerous authors. Several methods can be used to increase the functional range of angles through which light can be concentrated including multiplexing and cascading of multiple HOEs [11–13]. Holograms and their implementation into solar energy systems are explored in detail by Castro et al. [14] and Collados et al. [15], highlighting the potential, but also the need to design any system to minimise crosstalk and maximise the number of rays reaching the PV cell, as well as the importance of hologram orientation when considering its position in a solar collecting system.

HOEs have also found application in head-up displays with angular range being critical to ensure maximum field of view [16,17]. Recent developments show system designs achieving fields of view exceeding 60 degrees using an HOE with a diffracted beam that converges towards the eye of the viewer [18].

Applications are under development in HOE-based light management including projection systems [19] and diffusers for lighting applications (HELLA and Covestro present new designs for vehicle lighting) [20,21], among others [4].

Holographic recording in thinner layers is beneficial to applications where a low angular selectivity is an advantage. To accommodate the use of thinner layers, a good refractive index modulation (RIM) is required, so that high values of diffraction efficiency are still achievable, even though the path length through the grating is reduced. Thus, any improvements to the refractive index modulation that can be achieved in a given material can significantly improve performance and utility.

A key technical roadblock, at present, is that many of the existing holographic recording materials are very sensitive to environmental conditions such as humidity. This characteristic can be useful for making low-cost holographic sensors [22] and with the protection of a thin plastic cover layer, HOEs made in these materials can function well in many everyday applications. Some sensitive materials can be coated and sealed with a resistant plastic which reduces sensitivity and can block UV light from reaching the hologram [23]. However, in the context of solar concentration, outdoor lighting application and outdoor displays, any environmental sensitivity is detrimental. The ideal HOE should be unaffected by variables in its intended environment. Furthermore, the necessity for inclusion of resistant cover layers increases the final cost per HOE device and the complexity of the manufacturing process. Recently, a novel photopolymerisable hybrid sol–gel (PHSG) for holographic recording of both transmission and reflection volume gratings has been reported [24]. The material has significantly improved gelation time in comparison with other photopolymerisable glasses. One of the key strengths of this material is its excellent water resistance, with stable performance of the holographic gratings demonstrated following 400 h of complete immersion in water.

A subsequent investigation of the recording processes at 532 nm and UV curing has led to the fabrication of gratings that are up to 90% efficient in 118 μm thick layers (equivalent refractive index modulation approximately 0.002). These experimental results also confirm the capability to withstand temperatures up to 130 °C.

In this current study, we present further improvements to the refractive index modulation and recording sensitivity of this photosensitive sol–gel which has very high physical and environmental robustness and fast curing times.

2. Theoretical Background

2.1. Sol–Gel Chemistry

Sol–gel chemistry is a well-developed synthetic approach to fabricating new functional materials for applications in diverse areas such as medicine, pharmacy, mechanics, electronics, chemistry and others [25,26].

Photosensitive sol–gels are materials used for holographic recording, synthesised using sol–gel chemistry. Dry layers prepared from sol–gel solutions can have high optical quality, low scatter and scratch and water resistance. They can also be permanently optically patterned (thousands of L/mm) using a relatively low-intensity light source (typically a

few mW/cm^2). The aim of developing this material is to provide a holographic recording material with improved dimensional stability, robustness and capacity for making dry layers with thickness in the range from tens to hundreds of micrometers [27,28].

The photosensitive sol–gel utilised in this study represents a water-resistant photopolymerisable hybrid organic–inorganic sol–gel which belongs to Class II hybrid materials according to the classification proposed in [29]. These materials have covalent bonds between the organic and the inorganic species which provide improved dimensional stability and robustness. Dry photosensitive sol–gel layers achieved after thermal curing represent a xerogel consisting of nanoparticles made from MAPTMS with pores filled with transition metal inorganic complexes ((MAA:ZPO):ZCO) [24]. These nanoparticles are further cross-linked by (3-Aminopropyl)triethoxysilane (APTES). The stability of the xerogel, its robustness and the fine control over the pour size give the photosensitive sol–gel some distinct advantages over traditional photopolymer materials.

One of the roles of zirconium in the sol–gel's mechanism is to provoke the condensation of residual SI-OH groups in the acid catalysed hydrolysis reaction of MAPTMS into a more condensed silicate species. Adding more zirconium increases the number of Si-O-Zr bonds and the density of the overall hybrid system. This can decrease the porosity of the system [30]. When considered in the context of a photosensitive system intended for holographic recording, this increased density and reduced porosity can have different effects on the RIM depending on the recording method (or conditions) used.

It is hypothesised that the increased density of the sol–gel at higher zirconium concentrations may lead to a higher RIM, through variation in the background refractive index. It has been observed through theoretical modelling that a small variation in the binder background may cause a significant increase in the RIM achieved in holographic recording [31]. On the other hand, a larger density of the background matrix due to the reduced pore size may hinder any diffusion-related processes and thus have an adverse effect on the achieved RIM. The net effect will depend on the degree of diffusion that occurs during the patterning process, and as such, it is also of interest to study the same layers after thermal treatment. Thus, the effect of zirconium concentration and thermal treatment will be studied with the aim of improving the RIM of the photosensitive sol–gel material.

2.2. Photopolymerisation Mechanism

The photopolymerisation mechanism for holographic patterning of the photosensitive sol–gel is based on a free radical polymerisation process as follows. (1) Initiation: Under laser irradiation, the photoinitiator molecule (Irgacure 784) dissociates into free radicals that initiate further free radicals on the methacrylate groups (MAPTMS and MAA). (2) Propagation: The radicals produced on the methacrylate groups undergo polymerisation with neighbouring methacrylate groups, leading to the formation of rigidly structured nanoparticle-based species in illuminated areas and as a result a local change in the refractive index. If the illuminating light is appropriately patterned, this will lead to the creation of a diffraction grating. (3) Termination: A recombination reaction between two activated methacrylate groups (radicals) stops the polymerisation process.

2.3. Theoretical Modelling

The depth and period of modulation of the refractive index in the sol–gel depend on the characteristics of the light pattern that the material is exposed to, as well as the material's capability to change in response to the illumination. The characteristics of the recorded photonic structure determine the diffraction behaviour. Two of the most important considerations in the design of holographic devices are grating spatial frequency and thickness, because of their effects on the angular and chromatic selectivity of the device.

The ideal HOE (for many optical device-type applications) has just one single diffracted order and diffracts all of the incident light into the desired new direction, i.e., it has 100% diffraction efficiency in the first order.

Diffraction efficiency, η, is defined as the proportion of incident light intensity that is measured in a particular diffracted order. I_{+1} is the light intensity of the diffracted order and I_{in} is the intensity of the incident light.

$$\eta = \frac{I_{+1}}{I_{in}} \tag{1}$$

In a phase volume Bragg grating, the proportion of light diffracted depends on the phase difference introduced by the grating's spatially modulated refractive index. According to Kogelnik's coupled wave theory [3], the phase parameter V is defined as

$$V = \frac{\pi n_1 \, T}{\lambda \, \cos\theta_b}, \tag{2}$$

for a grating of thickness T with a refractive index modulation of n_1 and having a Bragg angle θ_b, at a particular wavelength λ [32].

Volume Bragg gratings are highly selective and the equation that relates diffraction efficiency to the Bragg angle detuning is:

$$\eta = \left[\frac{\sin\left(V^2 + E^2\right)^{\frac{1}{2}}}{\left(1 + \frac{E^2}{V^2}\right)^{\frac{1}{2}}} \right]^2 \tag{3}$$

where E is the off-Bragg parameter for an unslanted transmission phase grating, defined as

$$E_\theta = \frac{\Delta\theta \, 2\pi n \, T \, \sin\theta_b}{\lambda}. \tag{4}$$

Equation (4) shows that as we move away from the Bragg angle, the diffraction efficiency will drop much more rapidly for thick layers. In Equation (4), n is the average refractive index. This is advantageous in applications such as data storage and notch filters [33]. However, in many HOE applications it is desirable to minimise the thickness in order to maximise the angular and wavelength range at which one can have the HOE function efficiently as an optical element.

At the Bragg angle, since E is zero, the equation for diffraction efficiency reduces to Equation (5):

$$\eta = \sin^2\left[\frac{\pi n_1 \, T}{\lambda \, \cos\theta_b} \right]. \tag{5}$$

It is obvious from Equation (5) that high refractive index modulation and high thickness increase the (on-Bragg) diffraction efficiency.

The required refractive index modulation and diffraction efficiency η when probed at the Bragg angle θ_b are given in Equation (6):

$$n_1 = \frac{\sin^{-1}\sqrt{\eta}\,\lambda\cos\theta_b}{\pi T}. \tag{6}$$

As discussed above, the thickness of the hologram affects the operational range, both angular and wavelength [34], and for many applications (e.g., solar concentrators), expanding these operational ranges is critical. Thus, the development of thinner holograms is needed. If a diffraction efficiency close to 100% is to be achieved while simultaneously reducing the thickness of the hologram, there must be an increase in the refractive index modulation. This illustrates one of the challenges facing holographic concentrators: novel materials capable of large refractive index modulations which allow for thinner, less angularly selective holograms.

Of course, efficiency over a significant angular working range and spectral bandwidth are equally important in many HOE applications. Here, we model and measure only the

angular response for two reasons: (1) because it is the most experimentally reliable way to characterise and compare materials, i.e., using a fixed wavelength and varying angles, and (2) for transmission gratings, the angular range is much more likely to be the practical limiting factor.

Although thinner holograms are required, the thickness cannot be reduced indefinitely, or the grating ceases to behave as a Bragg grating. In order to redirect light in only one direction, the holograms must operate as a thick (volume) hologram. To ensure that the grating functions as a Bragg grating, the Q factor is often used to characterise the regime of operation of the device [34].

Holograms operate as volume holograms when the Q parameter is $\geq$10. Q is given by Equation (7).

$$\mathrm{Q} = \frac{2\pi\lambda T}{n\Lambda^2} \tag{7}$$

Q is dependent on the wavelength of the probing beam λ, the hologram thickness T, the average refractive index of the material n and the square of the period of the grating Λ. As shown schematically in Figure 1, angular selectivity (large operational range) will decrease as thickness and spatial frequency increase, and vice versa. Figure 2a illustrates the spatial frequency and thickness conditions required for a holographic grating to operate in the volume regime (indicated by the line at Q = 10).

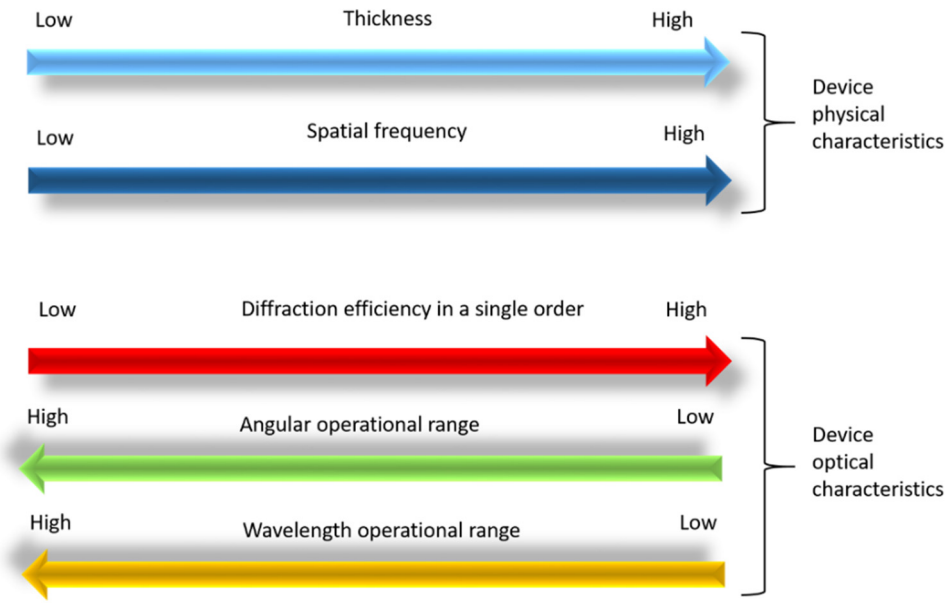

Figure 1. Relationship between the physical and optical characteristics of the hologram and their relevance to the design of the HOE.

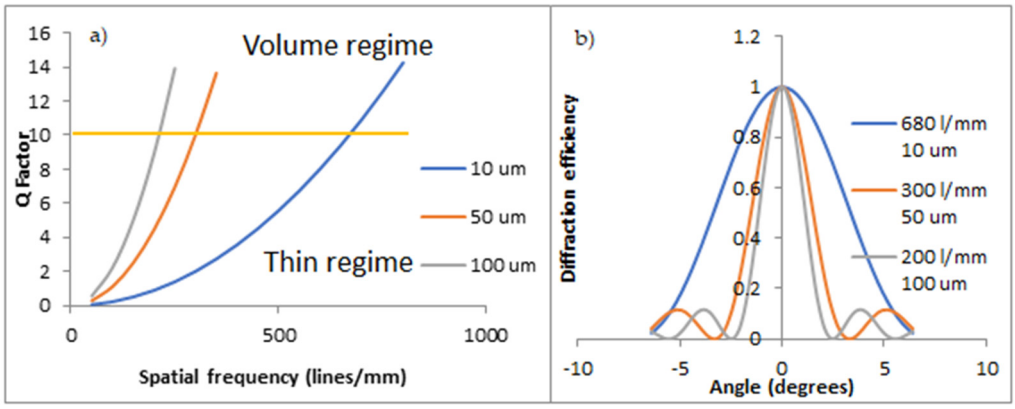

Figure 2. (**a**) Q factor at different grating thickness and spatial frequency values. (**b**) Angular selectivity curve at two different grating thicknesses and spatial frequencies with a Q factor of 10.

The Bragg curves in Figure 2b show the angular selectivity for three different spatial frequency and thickness combinations, that have a Q factor of 10; this clearly illustrates that lower angular selectivity (improved angular working range) can be more readily obtained using the combination of higher spatial frequency and lower thicknesses. Clearly, it is better to design for lower thicknesses, even if spatial frequency has to be raised, to keep Q at/above 10. Again, this is only valuable if the refractive index modulation of the material is high enough to achieve high diffraction efficiency in thinner layers. Figure 3 shows the refractive index modulation required for 100% diffraction efficiency for a range of thickness values. In each case, the spatial frequency that allows Q to equal 10 for that thickness is also given, as well as the indicative FWHM of the angular selectivity curve. Figure 3 demonstrates that raising the refractive index modulation enables reduced thickness which in turn enables a larger working range, but also indicates the lower spatial frequency limits associated with ensuring a single diffracted beam at each thickness.

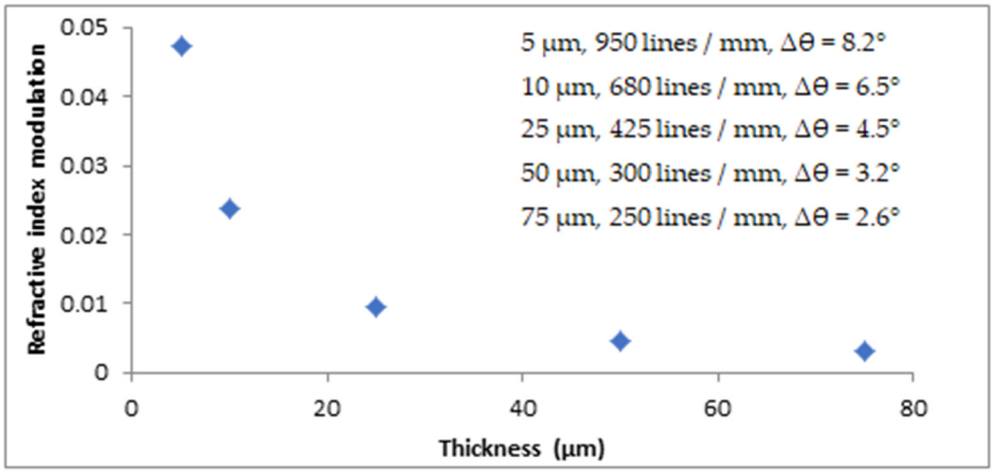

Figure 3. Refractive index modulation required at different layer thicknesses for achieving 100% diffraction efficiency, showing the spatial frequencies required at that thickness for Q = 10 along with the resulting full width half max angle (Δθ) of Bragg curve (angular selectivity).

3. Materials and Methods

3.1. Photosensitive Sol–Gel Preparation

The photosensitive sol–gel was synthesised by employing a four-step sol–gel process using two hybrid precursors: a trialkoxyorganosilane (3-trimethoxysilylpropyl methacrylate) and a zirconium complex prepared from the chelation of zirconium (IV) propoxide and methacrylic acid as described in detail in [24]. Briefly, 15 g (6.04×10^{-2} mol) of

3-trimethoxysilylpropyl methacrylate is mixed in a glass container with 0.8 g (4.44×10^{-2} mol) of aqueous nitric acid solution (0.1 M) for 45 min. At the same time, 0.727 g (2.218×10^{-3} mol) of zirconium (IV) propoxide is mixed with 0.13 g (1.567×10^{-3} mol) of methacrylic acid and is also stirred for 45 min. After both solutions have been prepared, they are then mixed together along with 1.08 g (6×10^{-2} mol) of deionised water for 24 h. This forms the base of the sol–gel and is illustrated in Figure 4.

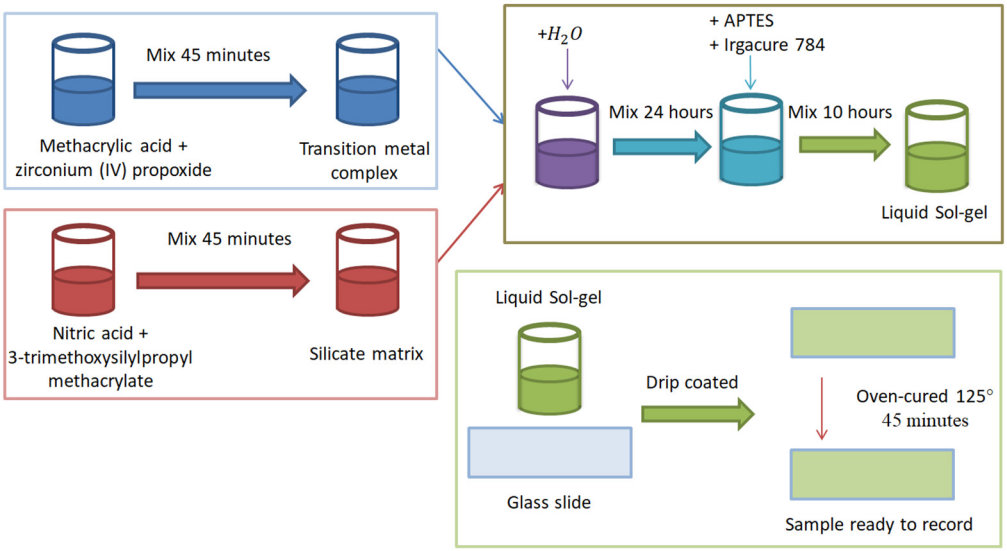

Figure 4. Illustration of the photosensitive sol–gel layer preparation procedure.

After the base is made, modification of the sol is carried out by adding (3-Aminopropyl) triethoxysilane (APTES) to improve the condensation ability of the hybrid nanoparticles during the gelation process and reduce the gelation time. Along with APTES, a photoinitiator Bis(eta.5-2,4-cylcopentadien-1-yl)-bis(2,6-difluoro-3-(1H-pyrrol-1-yl)-phenyl) titanium (Irgacure 784) is added to introduce photosensitivity in the blue–green wavelength region. So, 0.225 g of APTES (3.608×10^{-3} mol), 0.025 g (1.81×10^{-4} mol) of Irgacure 784 and 2 mL (2.617×10^{-2} mol) of isopropanol are added to 5 g of base. This is mixed for 24 h. Photosensitive layers are prepared by coating glass slides (76 mm × 26 mm) using a drip coating method. A pipette is used to measure 150–1000 mL of solution to achieve dry layer thicknesses of 15–100 µm, respectively. The samples are then put in an oven (Binder, model ED56) and cured at 125 °C for 45 min. The obtained dry layers are ready for recording.

3.2. Holographic Recording Set-Up

Holographic recording of volume phase transmission gratings was performed using a standard two-beam holographic recording geometry. Two lasers, either a 532 nm NDYAG laser or a 476 nm argon ion laser, were used as a light source in the holographic recording. The 532 nm recording arrangement is illustrated in Figure 5. The recording in the blue wavelength region was carried out with a similar set-up using the 476 nm line of an argon ion laser.

After the electronic shutter, the laser beam passes through a half wave plate followed by a polarising beam splitter, which allows easy adjustment of the beam ratio, to ensure high contrast in the interference pattern. The beam reflected by the polarising beam splitter is then spatially filtered, passed through an aperture and collimated before being reflected towards the photosensitive material in the sample holder. The other beam passes through another half wave plate to ensure both beams are in the same polarisation state (s-polarised), and then undergoes the same spatial filtering and collimation. Both beams overlap and interfere at the sol–gel sample in a sample holder with a spot size of 1 cm^2. A power meter records the power of a diffracted beam from a 633 nm probe beam (a wavelength to

which the material is not sensitive). The data are sent to a computer and real-time growth curves are generated as the grating is being recorded. A rotation stage on which the sample holder is mounted allows the same detector to also be used to generate Bragg selectivity curves. It should be noted that the diffraction efficiency figures were all obtained using an s-polarised 633 nm probe beam. In many real-world applications, however, the incident light is unpolarised. Diffraction efficiencies for unpolarised light will remain within 5% lower than that for s-polarised light, given that the spatial frequency of the grating is lower than 1000 L/mm. In addition, the modelling in this paper has been carried out for s-polarised light. For p-polarised components of the incident light, the phase term would be reduced by the cosine of twice the Bragg angle [2] and can be readily modelled. For large Bragg angles, such as those for coupler elements, a p-polarised probe beam can experience a significant drop in efficiency for a given refractive index modulation. For the results reported here (1000 and 500 L/mm gratings probed at 633 nm), the difference has been modelled and measured experimentally and is limited to a few percent (Supplementary Figure S2).

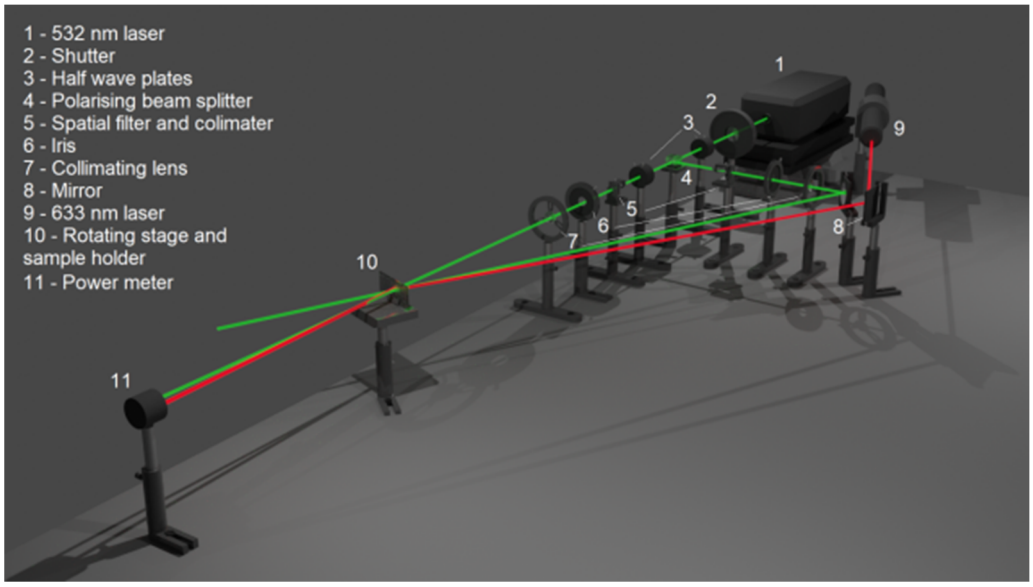

Figure 5. Holographic recording set-up.

3.3. UV–Vis Characterisation of the Recording Layers

A UV–Vis spectrum of dry photosensitive sol–gel layers on a glass substrate was obtained using a Perkin Elmer Lambda 900 UV/Vis/NIR Spectrometer to determine sensitivity at wavelengths between 325 and 800 nm in steps of 1 nm.

3.4. Thermal Processing

The heat treatment of photosensitive sol–gel samples was carried out using a fan-assisted oven (Binder, model ED56). This was used for dry layer preparation as detailed in Section 3.1, and for post-recording heat treatment.

4. Experimental Results

4.1. Characterisation of the Sol–Gel Layers for Holographic Recording

Since absorption of the recording light by the photosensitive layer is a crucial first step in the recording process, tuning the recording wavelength to better suit the absorption characteristics of the material is a key route to improved sensitivity. The UV–Vis spectrum of a photosensitive sol–gel layer was taken to determine its absorption at different laser recording wavelengths (Figure 6a).

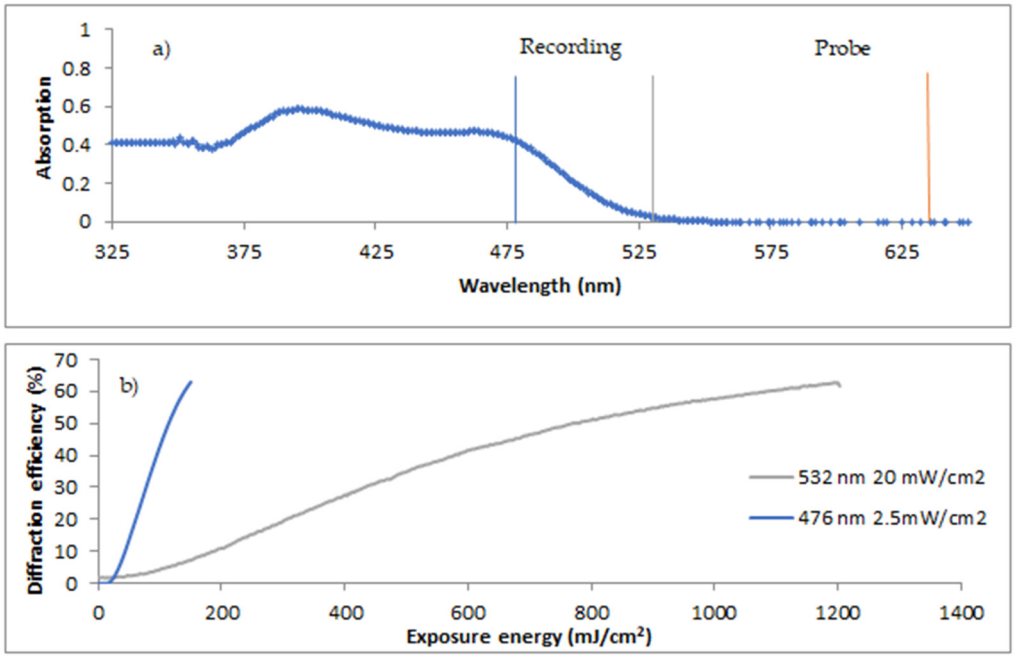

Figure 6. (**a**) UV–Vis spectrum of photosensitive sol–gel layers (after oven curing outlined in Figure 4) noting recording wavelengths of 532 and 476 nm, and probe wavelength of 633 nm; (**b**) diffraction efficiency growth curves of transmission gratings with the spatial frequency of 500 L/mm recorded at 532 nm and 476 nm with an intensity of 20 mW/cm^2 and 2.5 mW/cm^2, respectively; thicknesses for blue and green recordings are 80 and 100 µm, respectively.

The sol–gel absorption at 476 nm is 0.435, approximately 18 times higher than 0.023 for 532 nm. Although the recording processes are complex and absorption is only the first step, this information is useful when comparing the recording at the two different wavelengths and for determining the equivalent intensity to achieve equal photonic absorption independent of the wavelength used.

Figure 6b shows typical grating growth as a function of exposure energy for recording in green (532 nm) and in blue (476 nm) wavelength regions. The difference in exposure energy required for 50% diffraction efficiency (785 mJ/cm^2 for 532 nm vs. 114 mJ/cm^2 for 476 nm) confirms that the material absorbs much more efficiently at 476 nm; we can see an approximately 7-fold increase in sensitivity under these conditions. The final diffraction efficiency achieved was not significantly increased for any given layer thickness, however, the capacity to record with 7–8 times less intensity could confer a significant advantage in mass production.

4.2. Determination of the RIM and Its Dependence on Thickness of the Layers at 500/1000 L/mm

In order to find the upper limits of the RIM achievable with the photosensitive sol–gel, many holograms were recorded at both 532 and 476 nm at 500 and 1000 L/mm spatial frequencies and across a range of thicknesses from 18 to 380 µm. To avoid ambiguity, the Bragg selectivity curves of all samples were analysed and only values from samples that have not been over-modulated are included. The RIM achieved for individual samples was calculated by using Equation (6) and is presented in Figure 7.

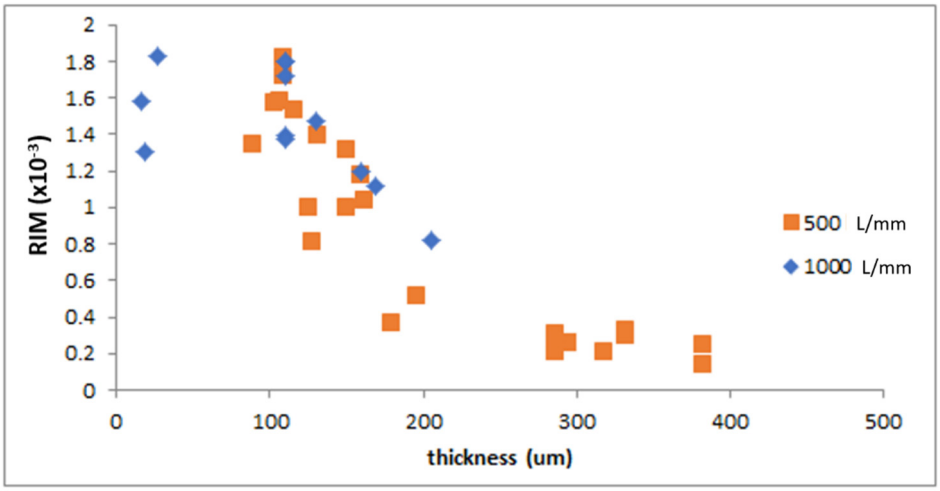

Figure 7. Maximum RIM achieved for individual samples with different thicknesses and spatial frequencies of 500 and 1000 L/mm.

In order to determine the RIM the sol–gel can achieve with this recording method, several more holograms were recorded in sample thicknesses below 100 µm. A 100 s recording time with a 476 nm laser and an intensity of 2.5 mW/cm^2 was used. An average RIM of $1.4 \times 10^{-3} \pm 1 \times 10^{-4}$ was achieved in layers with a thickness of 92 ± 11 µm over nine samples.

A few samples were recorded at a lower thickness than the others (15–25 µm), in order to determine if the RIM would continue to increase when layer thickness is below 100 µm. However, no increase in RIM was found at these thicknesses.

4.3. Effect of Zirconium Concentration

As mentioned above, a study of the zirconium concentration's effect on recording characteristics is of interest due to its effect on layer density. The addition of 2–9 times more zirconium (and methacrylic acid) to the sol–gel has proved to have a multitude of effects. One that is immediately observable is the exaggeration of an inhibition period at the beginning of holographic recording.

Effect of Zirconium Concentration on Grating Growth and RIM

Four example growth curves with different zirconium concentrations are shown in Figure 8a. As seen from Figure 8a, there is a period where, despite the recording beams illuminating the sol–gel, zero growth of the diffraction efficiency is observed. This inhibition period depends on the zirconium concentration, and it is longer for higher zirconium concentrations. Figure 8b shows the data for a wider range of concentrations and shows how the inhibition time changes linearly with zirconium concentration in this range.

For the highest concentration of zirconium, recording times of 5 min are required to reach the maximum diffraction efficiency. The overall sensitivity can be compared by measuring the time it takes to reach 10% diffraction efficiency: 300 s for 9 times the zirconium concentration compared to 6 s for 1 times concentration.

It should be noted that the addition of zirconium greater than 3 times the initial concentration increases the brittleness of the dry layers to a point where recording becomes ineffective. It was observed that layers with 3 times or less the initial zirconium concentration remain sufficiently plastic to form good stable layers. This physical change to the hardness of the material due to higher zirconium concentration may be a contributing factor to the observed inhibition times; along with the increased density that comes with high zirconium concentrations, it is possible mass transport becomes more limited.

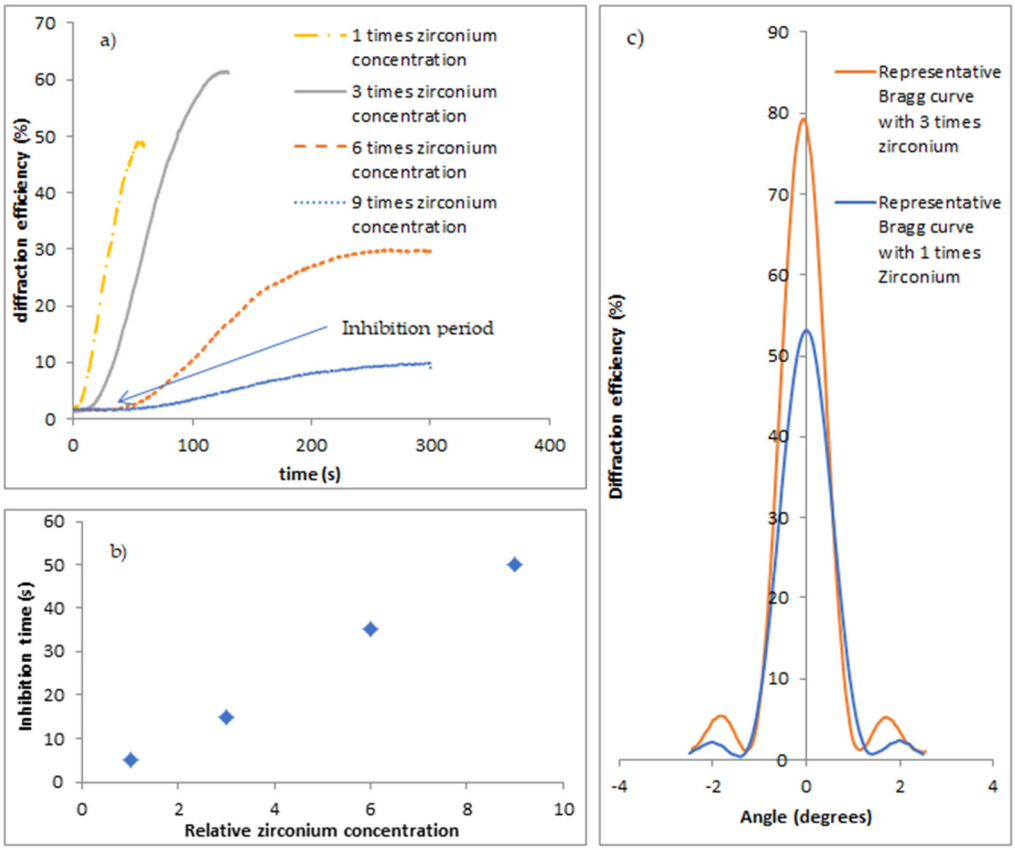

Figure 8. (**a**) Real-time diffraction efficiency growth curve for gratings recorded in photosensitive sol–gel with a 1, 3, 6 and 9 times increase in zirconium concentration (20 mW/cm^2, 532 nm, 1000 L/mm layer thickness ≈ 100 μm). (**b**) Inhibition time vs. relative zirconium concentration. (**c**) Representative Bragg curves for samples with 3 times zirconium concentration compared with the standard concentration (1 times). Samples recorded at 500 L/mm, 476 nm wavelength, 2.5 mW/cm^2 total recording intensity, 100 s exposure, ~80 μm thickness.

Several holographic gratings were recorded in order to determine the average RIM achieved when using 3 times the normal zirconium concentration. Two representative Bragg curves from the two thickness regimes chosen are shown in Figure 8c. The average RIM achieved over 23 samples in layers with 3 times the zirconium concentration at 500 L/mm was $1.9 \times 10^{-3} \pm 1 \times 10^{-4}$. This is a 36% increase over samples recorded with the standard zirconium concentration.

4.4. Thermal Treatment after a Short Exposure Time (Dark Processes)

It was observed that sol–gel samples exposed to the recording pattern for short periods (~10 s) would continue to develop in the absence of light. This dark process is shown in Figure 9, where after the initial exposure for 10 s the grating's diffraction efficiency increases from approximately 3% to 40–90% within 1800 s. This process on its own does not produce better results in terms of the final RIM; reaching values of $1.0 \times 10^{-3} \pm 1 \times 10^{-4}$, i.e., less when compared to fully exposed gratings. However, it does point towards the existence of processes with slower dynamics and their contribution to the recording process. It should be noted that this effect is most prominent in samples with the standard concentration of zirconium and less noticeable in higher zirconium concentration layers. This also points towards a light-driven process with fast dynamics (at these exposure conditions), followed by a dark process with relatively slower dynamics. Since the dark process was not observed as strongly in samples with additional zirconium, all experiments involving the dark process were carried out with the reference (1 times) zirconium concentration.

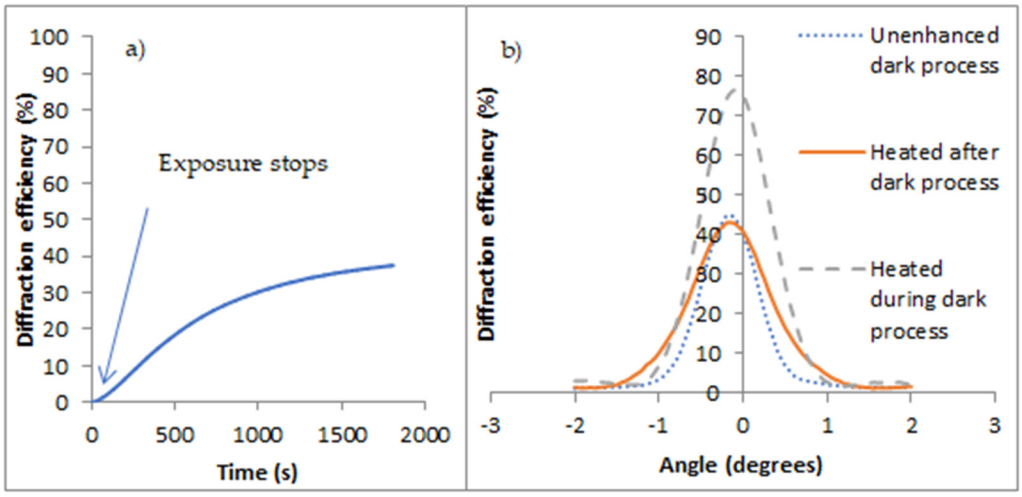

Figure 9. (**a**) Dark process growth curve of grating recorded using 10 s exposure, 476 nm, 2.5 mW/cm^2 total recording intensity; (**b**) Bragg curves of the grating treated by heat after the dark process had completed (solid), the grating heated during the dark process (dashed) and the grating with no heat treatment (dotted). Recorded at 532 nm, 1000 L/mm, 20 mW/cm^2, heat treated at 90 °C.

Figure 9a shows a real-time growth curve of a sol–gel sample developing through the dark process and Figure 9b shows the effect of thermal treatment during this period.

A few processes could be behind this dark process. The refractive index modulation may be increasing due to a continuation of chain polymerisation initiated during exposure, diffusion/mass transport of material as a result of the concentration difference set up by the consumption of material in the bright fringes; indeed, the dark process may be some combination of these effects., It was hypothesised that an increased temperature could assist in some chemical or physical process, as condensation reactions can be driven by catalysis and/or thermally [30]. So, it is possible that the thermal treatment of the sol–gel after recording may promote further condensation and a denser species and/or speed up diffusion, both of which could improve the RIM. The length of time it takes for the dark process to complete under these conditions made it practical to also examine the effect of temperature on the process observed in Figure 9a.

Samples were heat treated immediately after recording (during the dark process) for 30 min at different temperatures (60–110 °C) with a control sample that was heated after the dark process had already completed. Figure 9b shows how only the sample heated during the dark process experienced an increase in its diffraction efficiency. Samples heated above 80 °C during the dark process showed consistent improvement in the RIM compared to unheated samples. No notable difference was observed between samples heated at 80, 90 or 110 degrees (Supplementary Table S1).

Numerous samples were recorded at 500 L/mm and were heated immediately after exposure for 10 s. The average RIM of these samples was $2.6 \times 10^{-3} \pm 5 \times 10^{-4}$ with thicknesses of 65 ± 16 µm. Some of these samples became over-modulated as a result, so in order to determine the true limit to the RIM, the sample thickness was reduced and the spatial frequency increased to 1000 L/mm in order to stay in the volume regime.

For the thinner samples recorded at 1000 L/mm, the RIM had an average value of $3.3 \times 10^{-3} \pm 4 \times 10^{-4}$ in layers with an average thickness of 45 ± 13 µm. This represents an average increase due to heating of a factor of 2.4. The highest single value of RIM achieved was 4.2×10^{-3} (Supplementary Figure S1). This was measured in a sample heated at 90 degrees for 30 min during the dark process after 10 s exposure to a 532 nm laser at 20 mW/cm^2. The spatial frequency of recording was 1000 L/mm.

5. Discussion

The average RIM value has been improved using different methods. Producing holograms by exposing the sol–gel sample to the recording beams until the maximum diffraction efficiency was reached produced an average refractive index modulation of $1.4 \times 10^{-3} \pm 1 \times 10^{-4}$. Adding three times the amount of zirconium improved this value by 36% to $1.9 \times 10^{-3} \pm 1 \times 10^{-4}$. This improvement may be in part due to the denser sol–gel matrix that comes with increased zirconium concentrations. The relationship between zirconium concentration and material density is explored by Cullen et al. who showed that low zirconium concentrations lead to the formation of materials with lower densities [35].

Thermally treating sol–gel samples during the dark process at 90 °C for 30 min produced the highest RIM samples with an average value of $3.3 \times 10^{-3} \pm 4 \times 10^{-4}$ at 1000 L/mm, an improvement of a factor of three compared to unbaked samples. When this method of heating during the dark process is used on samples with 3 times the zirconium concentration, the effect of the heating on the RIM was slightly reduced, achieving a value of $2.8 \times 10^{-3} \pm 1 \times 10^{-4}$. It should also be noted that when comparing the RIM achieved during the dark process without thermal treatment (method 2), the sample with the higher zirconium concentration had lower RIM compared with samples with less zirconium. This can be explained by diffusion and/or polycondensation occurring after initial exposure. If diffusion contributes to the dark process, then the denser matrix that occurs when zirconium concentration is higher may hinder any mass transport through the pores of the matrix. The fact that sol–gel with higher zirconium concentration shows a smaller RIM increase during the dark process could also indicate that polycondensation is a contributor to the dark processes, since a more rigid structure (or sol–gel with higher zirconium concentration) has lower potential for densification of the network due to thermal curing.

The relative merits of the physical and chemical changes in improving RIM for samples described in Table 1 are shown in Figure 10. Table 2 summarises all the processes investigated here.

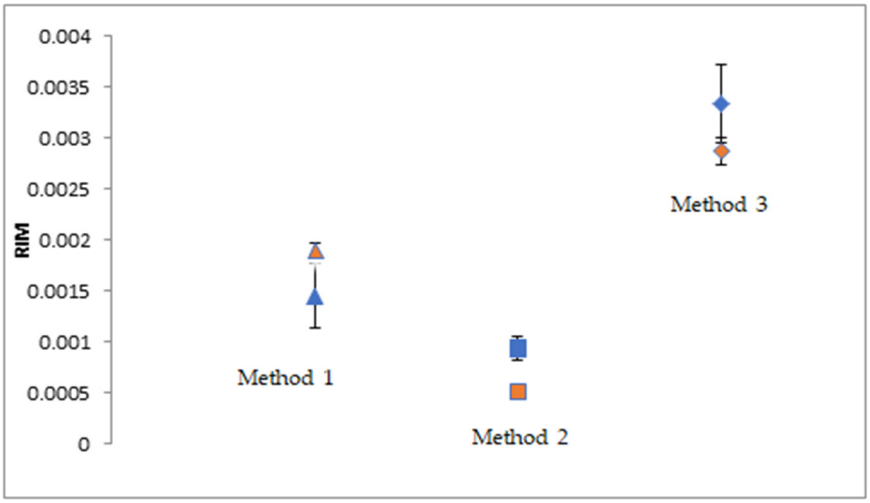

Figure 10. Average RIM values for each method of holographic recording as shown in Table 1. 1: Exposed to laser until full saturation of the diffraction efficiency growth, 2: Short exposure then allowed to complete dark process after, 3: Short exposure then thermally enhanced dark process at 90 °C, blue points for 1 times zirconium concentration and red points for 3 times zirconium concentration.

Table 1. Description of the recording conditions for samples in Figure 10.

Method	Details of the Sample
1	Exposed to laser until diffraction efficiency peaked (60–100 s exposure) (1000 lines/mm)
2	Exposed for 10 s and allowed to self-develop for 30 min (1000 lines/mm)
3	Exposed for 10 s and allowed to self-develop for 30 min at 90 degrees (1000 lines/mm)

Table 2. Summary of Results.

Change/Improvement	Sensitivity/Grating Growth Rate	RIM	Comment
Decreased the recording wavelength from green to blue	Increased 8-fold	Unchanged	
Decreased thickness of the layers	Not studied here	Improved RIM with thinner layers	More optimisation possible <100 microns
Increased zirconium concentration	Decreased	Increased 30–40%	
Post-exposure thermal treatment	Reduced exposure time to 1/10th	Final RIM improved by 300–400%	Heating immediately after exposure

6. Implications and Prospects

The work presented here is of course not an exhaustive study of all possible options or combinations, but it does provide a template and additional knowledge for tailoring the characteristics of this robust, durable, high optical quality material to suit desired specific applications. For example, chemical formulation changes (zirconium increase) can be used in most applications to achieve a higher RIM but at the cost of grating growth rate. This may better suit applications such as solar collectors [8,36,37] where RIM is crucial but a slower production rate is tolerable, compared to low-cost sensing devices [38–40], where lower RIM can be tolerated but high mass production rate is needed to drive down cost. The suitability of highly environmentally stable materials [24] for application in holographic sensors may seem counterintuitive, but in fact the insensitivity to variations in environmental humidity and temperature make it an ideal matrix to be functionalised for detection of a target analyte, without interference from the environmental conditions.

Better matching between recording wavelengths and the photosensitive material absorption properties very significantly increases the grating growth rate and improves production rates. This can be particularly useful in applications such as HOE TIR couplers [41] where the short wavelength enables recording without prisms; however, short wavelength lasers tend to be significantly more expensive at present, and the final RIM reached does not seem to be improved by recording in blue.

7. Conclusions

To conclude, a number of different methods have been explored, to the best of the authors' knowledge, for the first time with this sol–gel material, to improve its holographic recording properties and make it suitable for fabrication of HOEs for outdoor applications. An increase in the sensitivity by an order of magnitude was achieved by recording at a wavelength better matched to the material absorption spectrum. The refractive index modulation was improved by a factor of 2.4 by post-recording thermal treatment.

Heat treatment adds a production step to the process, but offers the promise of both shorter light exposure *and* significantly higher final RIM.

The average RIM value of $1.4 \times 10^{-3} \pm 1 \times 10^{-4}$ using typical holographic exposure methods has been improved to $3.3 \times 10^{-3} \pm 4 \times 10^{-4}$ using the thermal treatment method alone. A combination of different aspects of the above processes may improve this further to achieve the target RIM of 4×10^{-2}, as may a more detailed study of the recording dynamics and heating conditions.

Supplementary Materials: The following supporting information can be downloaded at: https://www.mdpi.com/article/10.3390/photonics9090636/s1, Figure S1: Bragg curve for an unslanted grating sample which achieved the highest RIM value (1000 l/mm 30 µm). Figure S2:Horizontally and vertically polarised probes at 633 and 532 nm of a 1000 l/mm thermally trated grating with standard zirconium concentration. The differnce between S and P polarised light is between 5 and 10 % diffraction efficiency. For this reason all gratings were probed with S polarised light; Table S1: Max RIM achieved by heating during dark process at different temperatures.

Author Contributions: Conceptualization, B.R., S.M. and I.N.; methodology, B.R., T.M., M.O., S.M. and I.N.; validation, T.M. and B.R.; formal analysis, B.R.; investigation, B.R.; supervision, I.N. and S.M.; writing—original draft preparation, B.R., S.M. and I.N.; writing—review and editing, B.R., T.M., D.C., S.M. and I.N. All authors have read and agreed to the published version of the manuscript.

Funding: B.R. would like to thank the Fiosraigh scholarship programme, TU Dublin for the financial support. All authors thank FOCAS, TU Dublin for the provided technical facilities and administrative support.

Institutional Review Board Statement: Not applicable.

Informed Consent Statement: Not applicable.

Data Availability Statement: Not applicable.

Conflicts of Interest: The authors declare no conflict of interest.

Abbreviations

HOE	Holographic optical element
RIM	Refractive index modulation
MAPTMS	3-trimethoxysilylpropyl methacrylate
MAA	Methacrylic acid
ZPO	Zirconium (IV) propoxide
ZCO	Zirconium complex
APTES	(3-Aminopropyl)triethoxysilane
L/mm	Lines per millimeter

References

1. Galli, P.; Evans, R.A.; Bertarelli, C.; Bianco, A. High fidelity holographic recording with cyclic allylic sulfide monomer. *Photosensit. Mater. Appl.* **2020**, *11367*, 1136711. [CrossRef]
2. Baldry, I.K.; Bland-Hawthorn, J.; Robertson, J.G. Volume Phase Holographic Gratings. Polarization Properties and Diffraction Efficiency. *Publ. Astron. Soc. Pac.* **2004**, *116*, 403–414. [CrossRef]
3. Kogelnik, H. Coupled wave theory for thick hologram gratings. *Bell Syst. Tech. J.* **1969**, *48*, 2909–2947. [CrossRef]
4. Bruder, F.K.; Fäck, T.; Rölle, T. The Chemistry and Physics of Bayfol® HX Film Holographic Photopolymer. *Polymers* **2017**, *9*, 472. [CrossRef] [PubMed]
5. Martin, S.; Akbari, H.; Keshri, S.; Bade, D.; Naydenova, I.; Murphy, K.; Toal, V. Holographically Recorded Low Spatial Frequency Volume Bragg Gratings and Holographic Optical Elements. In *Holographic Materials and Optical Systems*; Naydenova, I., Ed.; InTechOpen: London, UK, 2017; Chapter 4; pp. 73–98. ISBN 978-953-51-3038-3.
6. Wang, H.; Wang, J.; Liu, H.; Yu, D.; Sun, X.; Zhang, J. Study of effective optical thickness in photopolymer for application. *Opt. Lett.* **2012**, *37*, 2241–2243.
7. Bianco, G.; Ferrara, M.A.; Borbone, F.; Roviello, A.; Striano, V.; Coppola, G. Photopolymer-based volume holographic optical elements: Design and possible applications. *J. Eur. Opt. Soc. Rapid Publ.* **2015**, *10*, 15057. [CrossRef]
8. Marín-Sáez, J.; Atencia, J.; Chemisana, D.; Collados, M.V. Characterization of volume holographic optical elements recorded in Bayfol HX photopolymer for solar photovoltaic applications. *Opt. Express* **2016**, *24*, A720–A730. [CrossRef] [PubMed]
9. Neipp, C.; Francés, J.; Martínez, F.J.; Fernández, R.; Alvarez, M.L.; Bleda, S.; Ortuño, M.; Gallego, S. Optimization of Photopolymer Materials for the Fabrication of a Holographic Waveguide. *Polymers* **2017**, *9*, 395. [CrossRef]
10. Fernández, R.; Gallego, S.; Navarro-Fuster, V.; Neipp, C.; Francés, J.; Fenoll, S.; Pascual, I.; Beléndez, A. Dimensional changes in slanted diffraction gratings recorded in photopolymers. *Opt. Mater. Express* **2016**, *6*, 3455–3468. [CrossRef]
11. Naydenova, I.; Akbari, H.; Dalton, C.; Yahya, M.; Ilyas, M.; Pang Tee Wei, C.; Toal, C.; Martin, S. Photopolymer Holographic Optical Elements for Application in Solar Energy Concentrators. In *Holography—Basic Principles and Contemporary Applications*; Mihaylova, E., Ed.; InTechOpen: London, UK, 2013; pp. 129–145. ISBN 978-953-51-1117-7.

12. Akbari, H.; Naydenova, I.; Martin, S. Using Acrylamide Based Photopolymers for Fabrication of Holographic Optical Elements in Solar Energy Applications. *Appl. Opt.* **2014**, *53*, 1343–1353.
13. Keshri, S.; Marin-Saez, J.; Naydenova, I.; Murphy, K.; Atencia, J.; Chemisana, D.; Garner, S.; Collados, M.V.; Martin, S. Stacked volume holographic gratings for extending the operational wavelength range in LED and solar applications. *Appl. Opt.* **2020**, *59*, 2569–2579. [CrossRef] [PubMed]
14. Castro, J.M.; Zhang, D.; Myer, B.; Kostuk, R.K. Energy collection efficiency of holographic planar solar concentrators. *Appl. Opt.* **2010**, *49*, 858–870. [CrossRef] [PubMed]
15. Collados, M.V.; Chemisana, D.; Atencia, J. Holographic solar energy systems: The role of optical elements. *Renew. Sustain. Energy Rev.* **2016**, *59*, 130–140. [CrossRef]
16. Piao, J.A.; Li, G.; Piao, M.L.; Kim, N. Full Color Holographic Optical Element Fabrication for Waveguide-type Head Mounted Display Using Photopolymer. *J. Opt. Soc. Korea* **2013**, *17*, 242–248. [CrossRef]
17. Shen, Z.; Zhang, Y.; Weng, Y.; Li, X. Characterization and Optimization of Field of View in a Holographic Waveguide Display. *IEEE Photonics* **2017**, *9*, 1–11. [CrossRef]
18. Dimov, F.; Russo, J. Head-Mounted Display Having Volume Substrate-Guided Holographic Continuous Lens Optics with Laser Illuminated Microdisplay. U.S. Patent US20220099971A9, 31 March 2022.
19. Jackin, B.J.; Jorissen, L.; Oi, R.; Wu, J.Y.; Wakunami, K.; Okui, M.; Ichihashi, Y.; Bekaert, P.; Huang, Y.P.; Yamamoto, K. Digitally designed holographic optical element for light field displays. *Opt. Lett.* **2018**, *43*, 3738–3741. [CrossRef]
20. Automotive World Arcticle. HELLA and Covestro Present New Designs for Vehicle Lighting. October 2016. Available online: https://www.automotiveworld.com/news-releases/hella-covestro-present-new-designs-vehicle-lighting/ (accessed on 27 July 2022).
21. Murphy, K.; Toal, V.; Naydenova, I.; Martin, S. Holographic beam-shaping diffractive diffusers fabricated by using controlled laser speckle. *Opt. Express* **2018**, *26*, 8916–8922. [CrossRef]
22. Mikulchyk, T.; Walshe, J.; Cody, D.; Martin, S.; Naydenova, I. Humidity and temperature induced changes in the diffraction efficiency and the Bragg angle of slanted photopolymer-based holographic gratings. *Sens. Actuators B. Chem.* **2017**, *239*, 776–785. [CrossRef]
23. Rogers, B.; Martin, S.; Naydenova, I. Study of the Effect of Methyldiethanolamine Initiator on the Recording Properties of Acrylamide Based Photopolymer. *Polymers* **2020**, *12*, 734. [CrossRef]
24. Mikulchyk, T.; Oubaha, M.; Kaworek, A.; Duffy, B.; Lunzer, M.; Ovsianikov, A.; Gul, S.E.; Naydenova, I.; Cody, D. Synthesis of Fast Curing, Water-Resistant and Photopolymerizable Glass for Recording of Holographic Structures by One- and Two-Photon Lithography. *Adv. Opt. Mater.* **2022**, *10*, 2102089. [CrossRef]
25. Corriu, R.; Anh, N.T. *Molecular Chemistry of Sol-Gel Derived Nanomaterials*; Wiley: Chichester, UK, 2009.
26. Levy, D.; Zayat, M. *The Sol-Gel Handbook*; Wiley-VCH: Weinheim, Germany, 2015.
27. Carretero, L.; Murciano, A.; Blaya, S.; Ulibarrena, M.; Fimia, A. Acrylamide-N,N′-methylenebisacrylamide silica glass holographic recording material. *Opt. Express* **2004**, *12*, 1780. [CrossRef] [PubMed]
28. Schnoes, M.G.; Dhar, L.; Schilling, M.L.; Patel, S.S.; Wiltzius, P. Photopolymer-filled nanoporous glass as a dimensionally stable holographic recording medium. *Opt. Lett.* **1999**, *24*, 658. [PubMed]
29. Gomez-Romero, P.; Sanchez, C. *Functional hybrid Materials*; Wiley-VCH: Hoboken, NJ, USA, 2004.
30. Oubaha, M. *Introduction to Hybrid Sol-Gel Materials*; Volume 3, World Scientific Reference of Hybrid Materials; World Scientific Publishing Co.: Singapore, 2019.
31. Mackey, D.; O'Reilly, P.; Naydenova, I. Theoretical modeling of the effect of polymer chain immobilization rates on holographic recording in photopolymers. *JOSA A* **2016**, *33*, 920–929. [PubMed]
32. Toal, V. *Introduction to Holography*; CRC Press: London, UK, 2012.
33. Hesselink, L.; Orlov, S.S.; Bashow, M.C. Holographic data storage systems. *Proc. IEEE* **2004**, *92*, 1231–1280. [CrossRef]
34. Harihan, P. *Basics of Holography*; Cambridge University Press: Cambridge, UK, 2002.
35. Cullen, M.; O'Sullivan, M.; Kumar, A.M. The role of the hydrolysis and zirconium concentration on the structure and anticorrosion performances of a hybrid silicate sol-gel coating. *J. Sol-Gel Sci. Technol.* **2018**, *86*, 553–567.
36. Akbari, H.; Naydenova, I.; Ahmed, H.; McCormack, S.; Martin, S. Development and testing of low spatial frequency holographic concentrator elements for collection of solar energy. *Sol. Energy* **2017**, *155*, 103–109.
37. Chrysler, B.D.; Kostuk, R.K. Volume hologram replication system for spectrum-splitting photovoltaic applications. *Appl. Opt.* **2018**, *54*, 8887–8893. [CrossRef]
38. Branigan, E.; Martin, S.; Sheehan, M.; Murphy, K. Direct multiplexing of low order aberration modes in a photopolymer-based holographic element for analog holographic wavefront sensing. *Environ. Eff. Light Propag. Adapt. Syst. IV SPIE Remote Sens.* **2021**, *11860*, 27–38. [CrossRef]
39. Yetisen, A.K.; Naydenova, I.; Vasconcellos, F.D.C.; Blyth, J.; Lowe, C.R. Holographic sensors: Three-dimensional analyte-sensitive nanostructures and their applications. *Chem. Rev.* **2014**, *114*, 10654–10696. [CrossRef]
40. Naydenova, I. Holographic sensors. In *Optical Holography*; Blanche, P.-A., Ed.; Elsevier Inc.: Amsterdam, The Netherlands, 2020; ISBN 978-0-12-815467-0.
41. Fernandez, R.; Bleda, S.; Gallego, S.; Neipp, C.; Márquez, A.; Tomita, Y.; Pascual, I.; Beléndez, A. Holographic waveguides in photopolymers. *Opt. Express* **2019**, *27*, 827–840.